1ENTATION PAGE

Form Approved
OMB No. 0704-0188

1. AGENCY USE ONLY (Leave blank)	2. REPORT DATE	3. REPORT TYPE AND DATES COVERED
	4/20/93	Annual Report 8-1-92 to 7-31-93

4. TITLE AND SUBTITLE
(U) PARTICLE DISPERSION IN TURBULENT SPRAYS

5. FUNDING NUMBERS
PE - 61102F
PR - 2308
SA - BS
G - F49620-92-J-0418

6. AUTHOR(S)
IAN M. KENNEDY AND WOLFGANG KOLLMANN

7. PERFORMING ORGANIZATION NAME(S) AND ADDRESS(ES)
UNIVERSITY OF CALIFORNIA
DAVIS, CA 95616

8. PERFORMING ORGANIZATION REPORT NUMBER
AFOSR-TR- 93 0[illegible]

9. SPONSORING/MONITORING AGENCY NAME(S) AND ADDRESS(ES)
AFOSR/NA
Building 410
Bolling AFB DC 20332-6448

10. SPONSORING/MONITORING AGENCY REPORT NUMBER

11. SUPPLEMENTARY NOTES

12a. DISTRIBUTION/AVAILABILITY STATEMENT
Approved for public release; distribution is unlimited

12b. DISTRIBUTION CODE

13. ABSTRACT (Maximum 200 words)

Measurements of droplet dispersion and vaporization rates are carried out and compared with computational predictions. Droplet dispersion, mean axial velocity and the axial autocorrelation function of the droplets are measured using a laser sheet technique. The experimental facility is modified to accommodate a true spray using an ultrasonic atomizer and droplets injected with a fluorescent dye. The computational part of the project is the development of a Large Eddy Simulation method for the turbulent jet. A LES-model for the unresolved scales of the flow is implemented into the Navier-Stokes solver. The results for filtered and unfiltered variables are compared to the experiments and improvement of the particle statistics due to the LES-model is found.

14. SUBJECT TERMS	15. NUMBER OF PAGES
TURBULENCE, SPRAYS, PARTICLE DISPERSION	36
	16. PRICE CODE

17. SECURITY CLASSIFICATION OF REPORT	18. SECURITY CLASSIFICATION OF THIS PAGE	19. SECURITY CLASSIFICATION OF ABSTRACT	20. LIMITATION OF ABSTRACT
Unclassified	Unclassified	Unclassified	UL

PARTICLE DISPERSION IN A TURBULENT SHEAR FLOW

AFOSR Grant G-F49620-92-J-0418

Annual Report: 8/1/92 to 7/31/93.

Principal investigators: I.M. Kennedy and W. Kollmann

MAE Department, University of California at Davis, CA 95616

Research Objectives

The overall objective of the project is to test current modelling of droplet scale processes for spray combustion in a well defined turbulent shear flow by comparison of measurements of droplet dispersion and vaporization rates with computational predictions. Our specific goals in this year of the project were to measure the autocorrelation function of the axial velocity component of the droplets and to compare it with stochastic simulation results and the modification of the experimental facility to accommodate a true spray using an ultrasonic atomizer and droplets injected with a fluorescent dye.

The computational phase of the project is aimed at the development of a Large Eddy Simulation method for the turbulent jet that has been the object of the experimental study. The goal is to obtain a simulation of the jet under conditions that match the experimental conditions so that droplet dispersion and vaporization rates can be compared and correlations of drag and mass transfer evaluated. Our specific goal in this year of the project was to implement a LES-model for the unresolved scales of the flow into the Navier-Stokes solver and to compare the filtered and unfiltered results to evaluate the effect on particle dispersion and vaporization rates.

Research Accomplishments

Experimental

One of the major unknowns in modeling particle dispersion in turbulent flows is the form of the Lagrangian velocity autocorrelation function for fluid and discrete particles. If this function is known, then it is possible to obtain the dispersion i.e., the mean square displacement from a known initial point. Snyder and Lumley (1971) obtained the autocorrelation function in a grid-generated turbulence but there are no data for particles in a turbulent shear flow such as a jet. One phase of the project over the last year has been devoted to obtaining this fundamental information.

The basic experimental methodology has been reported elsewhere (Call and Kennedy, 1991, 1992). A laser sheet is formed with cylindrical lenses. Droplets are issued from a piezoelectric generator into the jet near the centerline of the jet pipe exit. As a droplet passes through the laser sheet, the scattered radiation is collected and imaged onto a position-sensing photomultiplier tube. This scheme has been modified to obtain velocity and correlation information. Two sheets of parallel light are produced with a beam splitter and right angle prism. The parallel sheets are reflected back across the jet with a retroreflector with an adjustable spacing between the pairs of laser sheets. The time between scattering spikes from each sheet yields droplet velocity data, whatever the droplet location across the jet cross-section. Autocorrelations of the axial particle velocity can be obtained from the two velocity measurements from the two pairs of sheets. The autocorrelations can be reported in either an Eulerian form as a function of spatial separation or in a quasi-Lagrangian form as a function of time from the first transit through the first set of laser sheets.

We have studied hexadecane droplets ranging in diameter from 50 μm to 35 μm. In addition, hollow glass spheres of 40 μm diameter have been used to approximate fluid particles. Figure 1 shows the quasi-Lagrangian autocorrelation function for axial particle velocity at a number of axial locations along the jet. The correlations approximate exponential functions quite well. Insufficient data are available at longer times to comment on

the applicability of other functions, such as the Frenkiel function. The Stokes number of the particles has a clear impact on the correlation function. The turbulence Stokes number (based on a fluid integral length scale) is 0.16 and 0.33 for the 35 and 50 micron droplets respectively.

Comparisons with a stochastic simulation have emphasized the difficulty inherent in the prescription of length and time scales in turbulent flows with a one-point closure model. The stochastic simulation under predicts the integral length scale for droplet motion by a factor of two. Of course, the model constant that prescribes the eddy life time could be adjusted but there is little a priori guidance for the choice of this value.

Droplet dispersion measurements have been carried out during the last year with varying jet Reynolds number. The Reynolds number is changed by adjusting the nozzle diameter and the jet exit velocity to study the effect of the turbulent length and time scales on droplet dispersion. Typical Reynolds numbers are Re = 10000, 20000, and 30000 obtained with the nozzle diameters $D = 7mm$, $10mm$, and $12.6mm$. Figure 1 shows the average axial velocity and the root mean square value of the axial velocity fluctuations at the three different Reynolds numbers. The turbulent flow at the higher Reynolds numbers will also create noticable radial velocities for the larger ($90\mu m$) droplets making its measurement possible and facilitating the study of the effect of the turbulent scales on their dispersion.

The experimental facility is being modified to accommodate a true spray. Figure 2 shows the experimental set up for the spray simulation. An ultrasonic atomizer has been installed in a chamber to provide a fine spray with droplet diameters from 20 to 80 μm. The ultrasonic atomizer offers the advantage of very low air flow rates so that the flow of air in the experiment is not greatly disturbed. Single droplets that contain a fluorescent dye will be injected by the piezoelectric generator onto the centerline of the spray. A holographic edge filter will remove the Mie scattering from the spray. The fluorescence from the dye-containing droplet will be detected by the position-sensing photomultiplier tube as before. We plan to study the impact of dispersed phase loading in the spray on droplet dispersion with this system.

Theory and Computation.

Direct simulation of turbulent round jets is still not within the capabilities of present computers (Reynolds, 1990). Hence, Large Eddy Simulation of the turbulence in round jets is the most realistic approach for the prediction of the flow field and truly Lagrangian particle dynamics. The simulation of turbulent flow fields in round jets is based on accurate finite-difference methods, which offer the flexibility necessary for the treatment of non-periodic jet flows emitting from nozzles and the consideration of a variety of exit conditions. This aspect of the project was described in detail in the final report for grant AFOSR 89-0392 and further details can be found in Lienau, Kennedy and Kollmann (1993) and Lienau and Kollmann (1993) of the publication list. Two new contributions were accomplished during the period 1992-3. The numerical treatment of the coordinate axis $r = 0$ for unsteady flows without symmetries was analyzed (details in the appendix) and a satisfactory method was found to avoid the loss of accuracy near the axis. The second and main contribution was the implementation of a LES-model for the non-resolved scales of the turbulence. The Navier-Stokes equations are written for filtered variables

$$\bar{f}(\underline{x},t) \equiv \int d\underline{x}' G(\underline{x}-\underline{x}',t) f(\underline{x}',t) \tag{1}$$

where $G(\underline{x}-\underline{x}',t)$ denotes the filter function and $f(\underline{x},t)$ a dependent variable. The Navier-Stokes equations (in Cartesian coordinates for convenience) are filtered and emerge as

$$\frac{\partial \bar{v}_\alpha}{\partial x_\alpha} = 0 \tag{2}$$

and

$$\frac{\partial \bar{v}_\alpha}{\partial t} + \frac{\partial}{\partial x_\beta}(\bar{v}_\alpha \bar{v}_\beta) = -\frac{1}{\rho}\frac{\partial \bar{P}}{\partial x_\alpha} + \nu \frac{\partial^2 \bar{v}_\alpha}{\partial x_\beta \partial x_\beta} - \frac{\partial}{\partial x_\beta}(L_{\alpha\beta} + C_{\alpha\beta} + R_{\alpha\beta}) \tag{3}$$

The modified filtered pressure is defined by

$$\bar{P} \equiv \bar{p} + \frac{1}{3}\rho \delta_{\alpha\beta} \overline{v'_\alpha v'_\beta} \tag{4}$$

and the correlations of filtered and sub-grid-scale motion ($v'_\alpha = v_\alpha - \bar{v}_\alpha$) are given by

$$L_{\alpha\beta} \equiv \overline{\bar{v}_\alpha \bar{v}_\beta} - \bar{v}_\alpha \bar{v}_\beta \tag{5}$$

$$C_{\alpha\beta} \equiv \overline{v'_\alpha \bar{v}_\beta} + \overline{\bar{v}_\alpha v'_\beta} \tag{6}$$

$$R_{\alpha\beta} \equiv \overline{v'_\alpha v'_\beta} - \frac{1}{3}\delta_{\alpha\beta}\overline{v'_\gamma v'_\gamma} \tag{7}$$

The present filter is the top hat filter and the closure for the correlations is given by

$$L_{\alpha\beta} + C_{\alpha\beta} \doteq 0 \tag{8}$$

and the Smagorinsky model for $R_{\alpha\beta}$ (Reynolds, 1990)

$$R_{\alpha\beta} \doteq -2\nu_T S_{\alpha\beta} \tag{9}$$

where the eddy-viscosity is defined by

$$\nu_T \equiv (c\Delta)^2 (2S_{\alpha\beta}S_{\alpha\beta})^{\frac{1}{2}} \tag{10}$$

and

$$\Delta \equiv (\Delta x \Delta y \Delta z)^{\frac{1}{3}} \tag{11}$$

and

$$S_{\alpha\beta} \equiv \frac{1}{2}\left(\frac{\partial \bar{v}_\alpha}{\partial x_\beta} + \frac{\partial \bar{v}_\beta}{\partial x_\alpha}\right) \tag{12}$$

is the rate of strain produced by the filtered velocity field.

The result of modelling the sub-grid-scale motion is shown in fig.3 to fig.9. The turbulent flow in the round jet of the experiments by Call and Kennedy (1991) at the nominal Reynolds number of $Re = 15.000$ is calculated for $0 \leq \frac{x}{D} \leq 60$ without the LES-model, where the discretiztion error plays the role of the filter (Boris,1990), and with the Smagorinsky model discribed above. The vorticity magnitude for the former case is shown in fig.3 and in fig.4 for the latter case. It is evident that the LES-model using the eddy viscosity (10) dampens the smaller scales and reduces the scale range. It turns out that the spreading rate in the LES case is in very good agreement with the experimental evidence. More importantly, the effect of the LES-model on the particle statistics is also beneficial as the following figures prove. The dispersion of $113\mu m$ pentane particles in the heated jet (temperature difference at jet pipe exit: $60^o K$) as function of the axial distance

in fig.5 shows excellent agreement between measurement and numerical simulation with the LES-model. Preliminary results for the auto-correlation function of the axial velocity component of lighter ($50\mu m$ hexadecane) particles in fig.6 shows also close agreement with the experiments of Call and Kennedy (1991). The calculation of the time of flight plays a noticable role for dispersion as fig.7 illustrates. The experiment is limited to the mean time of flight wheras the numerical simulationm allows the computation of individual times of flight. It is evident from fig.7 that the dispersion calculated with the experimental (mean) time of flight is much closer to the measurements. The effect of the LES-viscosity on the dispersion is shown in fig.8. The increase in viscosity due to the LES-model (10) decreases the dispersion and improves the agreement with the measurements. Finally, mean particle velocity in axial direction is fairly independent of the method of calculating the time of flight as fig.9 shows.

References

Boris, J.P. (1990), "Comments on subgrid turbulence models and large eddy simulations", in *Whither Turbulence? or Turbulence at the Crossroads* (J.L. Lumley ed.), Lecture Notes in Physics vol. 357, Springer V., 344

Call, C.J. and Kennedy, I.M. (1991), "A technique for measuring Lagrangian and Eulerian particle statistics in a turbulent flow", Exper. in Fluids **12**, 125.

Call, C.J. and Kennedy, I.M. (1992), "Droplet dispersion, velocity and vaporisation in heated and unheated jets", Paper No. 92-42 Spring Meeting of the Western States Section of the Combustion Institute, Corvallis OR, March 1992.

Reynolds, W.C. (1990), "The potential and limitations of direct and large eddy simulations", in *Whither Turbulence? Turbulence at the Crossroads*, (J.L. Lumley ed.), Lecture Notes in Physics no. 357, Springer V., 313.

Snyder, W.K. and Lumley, J.L. (1971), "Some measurements of particle velocity autocorrelation functions in a turbulent flow", J. Fluid Mech. **48**, 41.

2.0 Personnel.

I. M. Kennedy	P. I.	15% time
W. Kollmann	Co - P. I.	15% time
J. J. Lienau	Ph. D. candidate	25% time
M. H. Moody	Master student	25% time

3.0 Publications.

Call, C.J. and Kennedy, I.M. (1990), "Particle dispersion ina turbulent shear flow", AIAA Paper 90-0468, AIAA Aerospace Sciences Meeting, Reno NV.

Call, C.J. and Kennedy, I.M. (1991), "A technique for measuring Lagrangian and Eulerian particle statistics in a turbulent flow", Exper. in Fluids **12**, 125.

Call, C.J. and Kennedy, I.M. (1991), "Particle dispersion and velocity statistics in a turbulent shear flow: Measurements and simulations", Paper No. 91-38 Spring Meeting of the Western States Section of the Combustion Institute, Boulder CO, March 1991.

Call, C.J. and Kennedy, I.M. (1992), "Droplet dispersion, velocity and vaporisation in heated and unheated jets", Paper No. 92-42 Spring Meeting of the Western States Section of the Combustion Institute, Corvallis OR, March 1992.

Hansell, D., Kennedy, I.M. and Kollmann, W. (1992), "A simulation of particle dispersion in a turbulent jet", J. Multi-Phase Flow **18**, 559-576.

Call, C.J. and Kennedy, I.M. (1993), "Droplet dispersion, velocity and vaporization in heated and unheated jets", AIAA 93-0904.

Call, C.J. and Kennedy, I.M. (1993), "Measurements of droplet dispersion in heated and unheated turbulent jets", to appear in AIAA Journal.

Lienau, J.J., Kennedy, I.M. and Kollmann, W. (1993), "Numerical simulation of particle dispersion in turbulent jets", AIAA 93-0547.

Lienau, J.J. and Kollmann, W. (1993), "Numerical simulation of the turbulent flow in round jets", AIAA 93-0199.

Lienau, J.J. and Kollmann, W. (1993), "Numerical simulation of propagating surfaces in turbulent plane jets", AIAA 93-3119.

4.0 Presentations.

Papers based on work for this project have been delivered in the following venues:

1992:

Fall meeting of the Western States Section of the Combustion Institute.

1993:

(1) AIAA Aerospace Sciences Meeting, Reno NV, Jan. 1993.

(2) AIAA 24th Fluid Dynamics Conference, Orlando FL, July 1993.

5.0 Interactions.

This work has been presented at the AIAA meetings and the Meetings of the Western States Section of the Combustion Institute.

Inventions.

None

Figure captions

vskip 12pt Fig.1 Axial mean velocity and the rms value of the axial velocity fluctuations at several Reynolds numbers.

Fig.2 Experimental set up for spray droplet dispersion.

Fig.3 Vorticity magnitude in planes $\theta = 0$ and $\theta = \pi$ at dimensionless time $t = 898$ and a $62 \times 16 \times 190$ grid for the flow in a round jet ($Re = 15000$) without the LES-model.

Fig.4 Vorticity magnitude in planes $\theta = 0$ and $\theta = \pi$ at dimensionless time $t = 870$ and a $62 \times 16 \times 190$ grid for the flow in a round jet ($Re = 15000$) with the LES-model.

Fig.5 Dispersion of $113\mu m$ vaporizing pentane particles in a heated jet as function of axial distance obtained with the LES model ($c_s = 0.05$, full line) compared to the experiments of Call and Kennedy (1991, broken line).

Fig.6 Auto-correlation function for the axial velocity of $50\mu m$ hexadecane particles in an unheated jet as function of the mean time of flight (Full line: Numerical simulation with the LES model, broken line: Experiment of Call and Kennedy, 1991).

Fig.7 Dispersion of $113\mu m$ vaporizing pentane particles in a heated jet as function of time. The numerical results were obtained with the LES-model and the time of flight was calculated using the true Lagrangean time of flight (full line) and the mean time of flight (broken line) as in the experiments of Call and Kennedy (1991, dotted line).

Fig.8 Dispersion of $113\mu m$ vaporizing pentane particles in a heated jet as function of the mean time of flight obtained without the LES model ($c_s = 0.0$, full line), with the LES-model ($c_s = 0.025$, broken line) compared to the experiments of Call and Kennedy (1991, dotted line).

Fig.9 Mean axial velocity of $113\mu m$ pentane particles in a heated jet as function of the mean time of flight obtained with the LES-model (full line: True Lagrangean time, broken line: Mean time of flight).

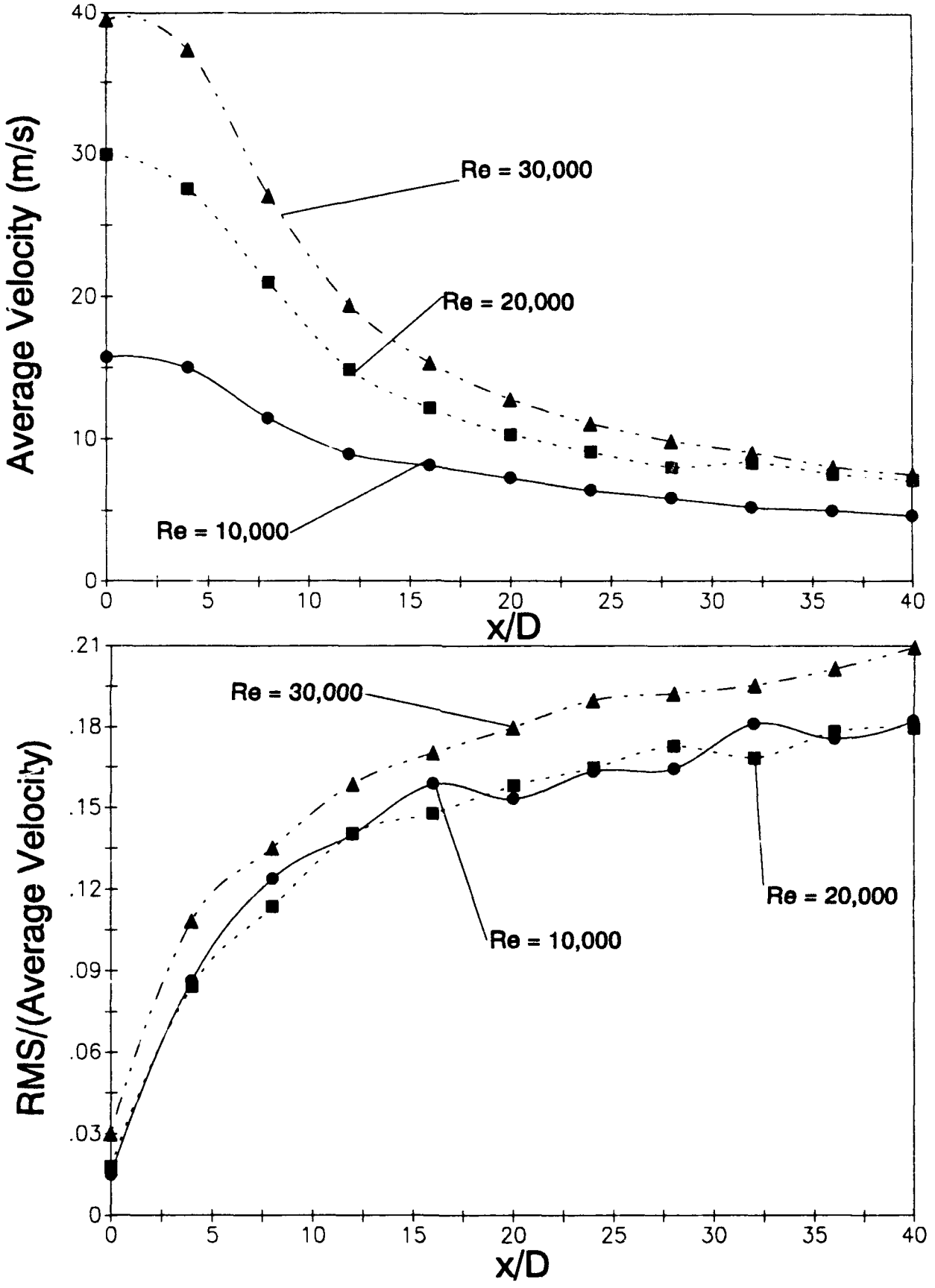

Axial Velocity and Root Mean Square Profiles for
Different Reynolds Number. Nozzle Diameter = 10mm.

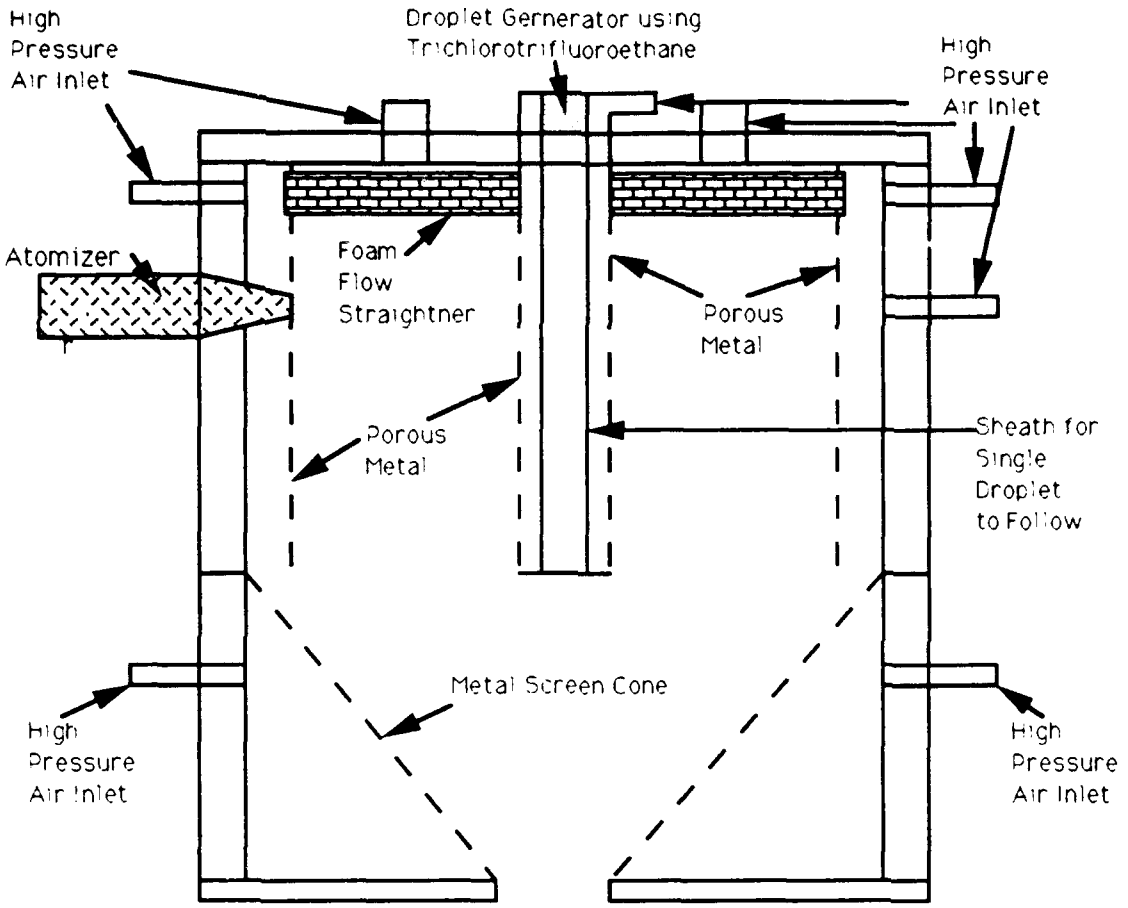

Figure 2. Experimental Apparatus for Spray Droplet Dispersion

VORTICITY MAGNITUDE

60 D UNLV Run

18 D in Radius

CONTOUR LEVELS

0.00000
0.05000
0.10000
0.15000
0.20000
0.25000
0.30000
0.35000
0.40000
0.45000
0.50000
0.55000
0.60000
0.65000
0.70000
0.75000
0.80000
0.85000
0.90000
0.95000
1.00000
1.05000
1.25000
1.30000
1.35000
1.40000
1.45000
1.50000
1.55000
1.60000
1.65000
1.70000
1.75000
1.80000
1.85000
1.90000
1.95000
2.00000
2.05000
2.10000

0.071	MACH
0.00 DEG	ALPHA
7.50x10**3	Re
8.98x10**2	TIME
62 x 16 x 190	GRID

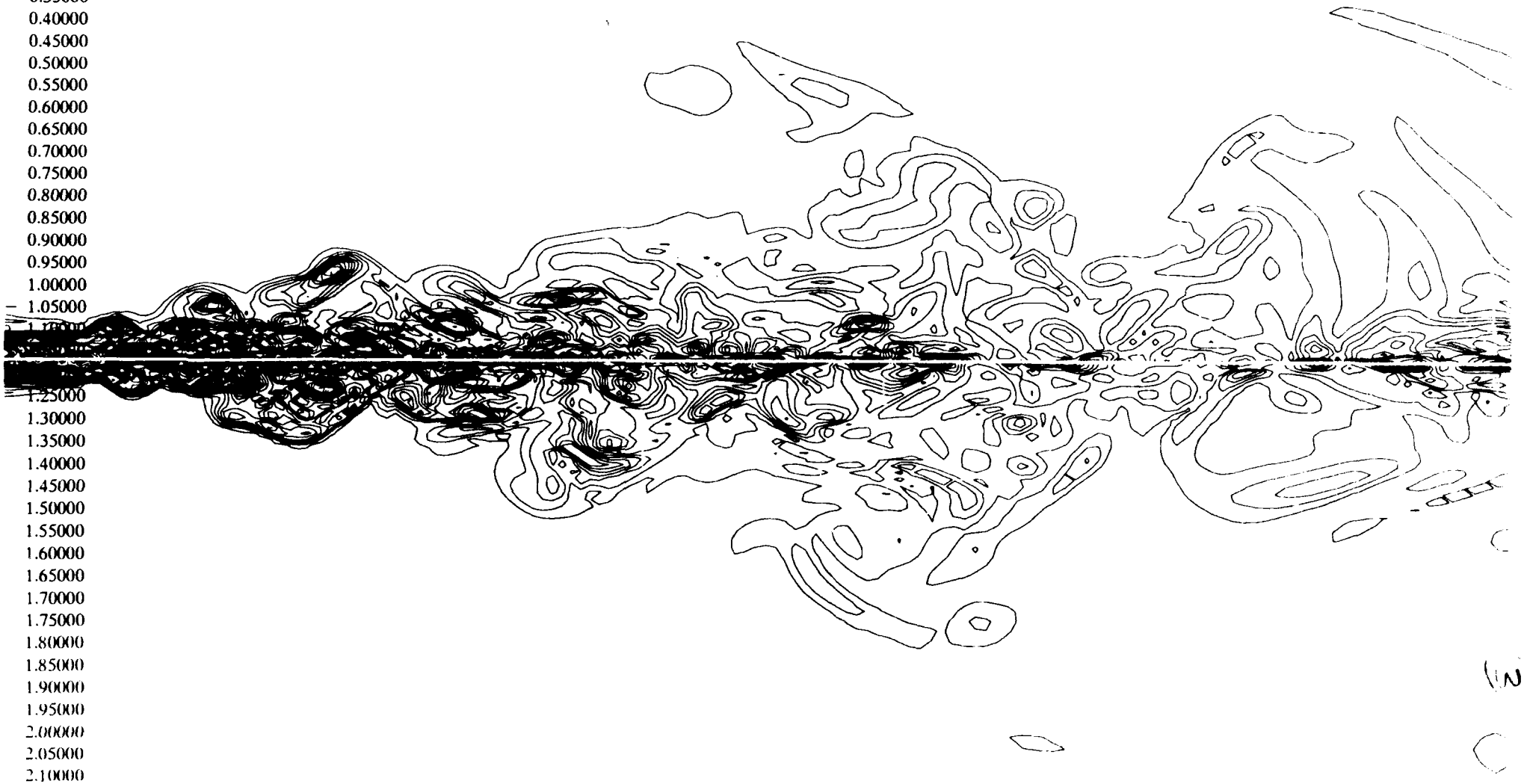

VORTICITY MAGNITUDE

60 D UNLV LES run

Cs=0.025, 18 D in radius

CONTOUR LEVELS

0.00000
0.10000
0.20000
0.30000
0.40000
0.50000
0.60000
0.70000
0.80000
0.90000
1.00000
1.10000
1.20000
1.30000
1.40000
1.50000
1.60000
1.70000
1.80000
1.90000
2.00000
2.10000
2.20000
2.30000
2.40000
2.50000
2.60000
2.70000
2.80000
2.90000
3.00000
3.10000
3.20000
3.30000
3.40000
3.50000
3.60000
3.70000
3.80000
3.90000
4.00000
4.10000
4.20000

0.069	MACH
0.00 DEG	ALPHA
7.50x10**3	Re
8.70x10**2	TIME
62 x 16 x 190	GRID

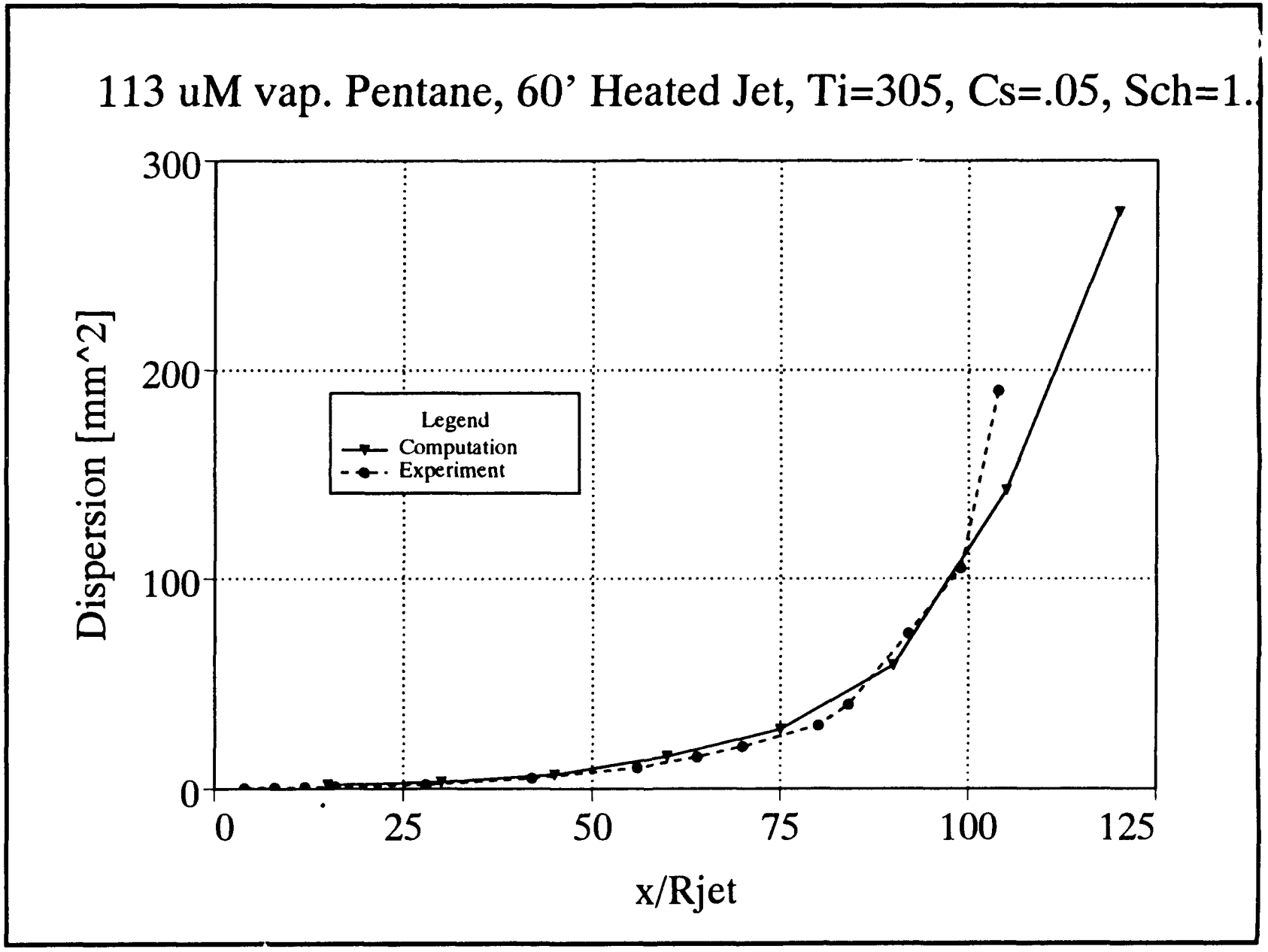
113 uM vap. Pentane, 60' Heated Jet, Ti=305, Cs=.05, Sch=1.
Dispersion [mm^2]
300
200
100
0
0
25
50
75
100
125
x/Rjet
Legend
Computation
Experiment

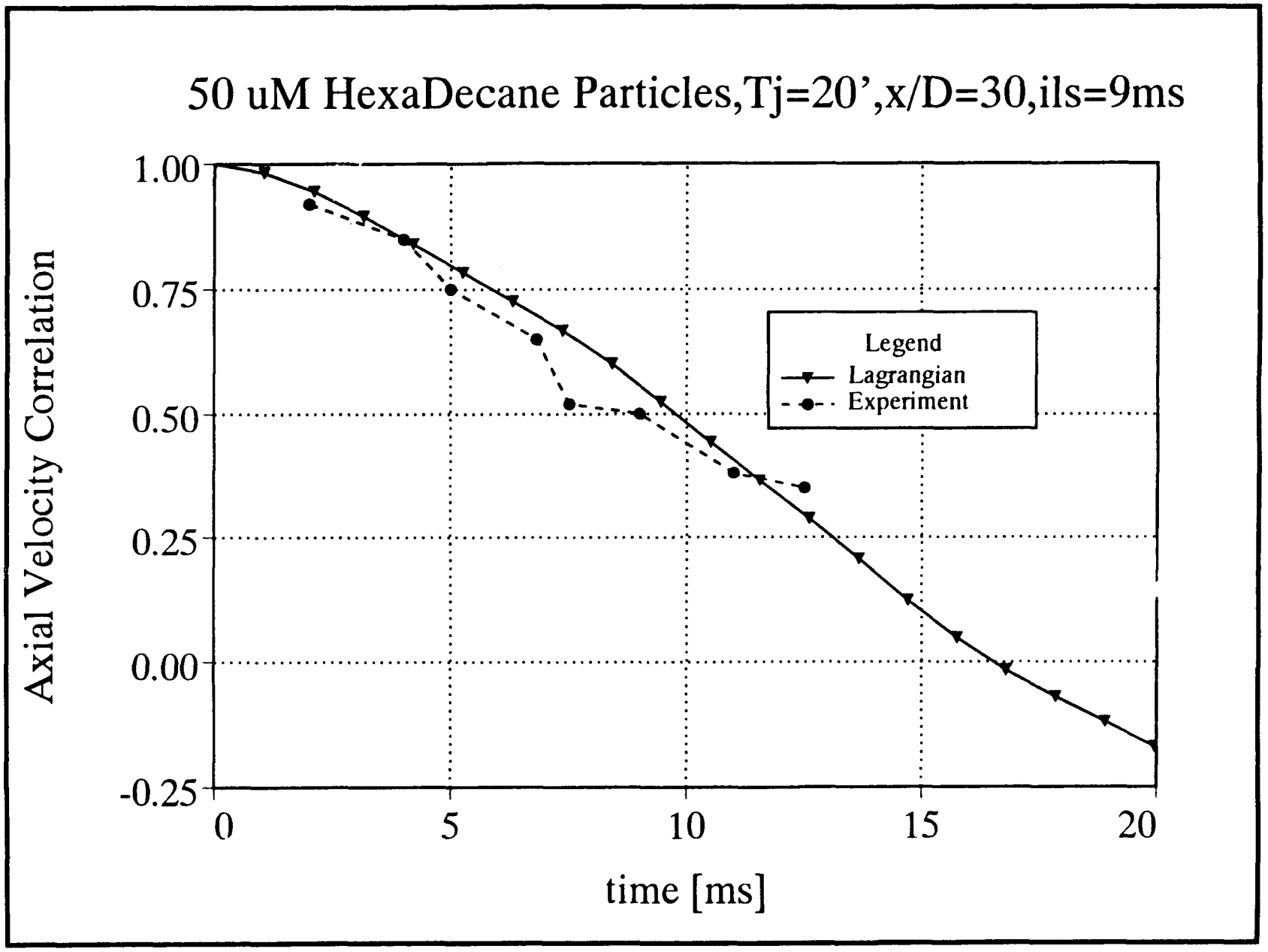
50 uM HexaDecane Particles,Tj=20',x/D=30,ils=9ms
Axial Velocity Correlation
1.00
0.75
0.50
0.25
0.00
-0.25
0
5
10
15
20
time [ms]
Legend
Lagrangian
Experiment

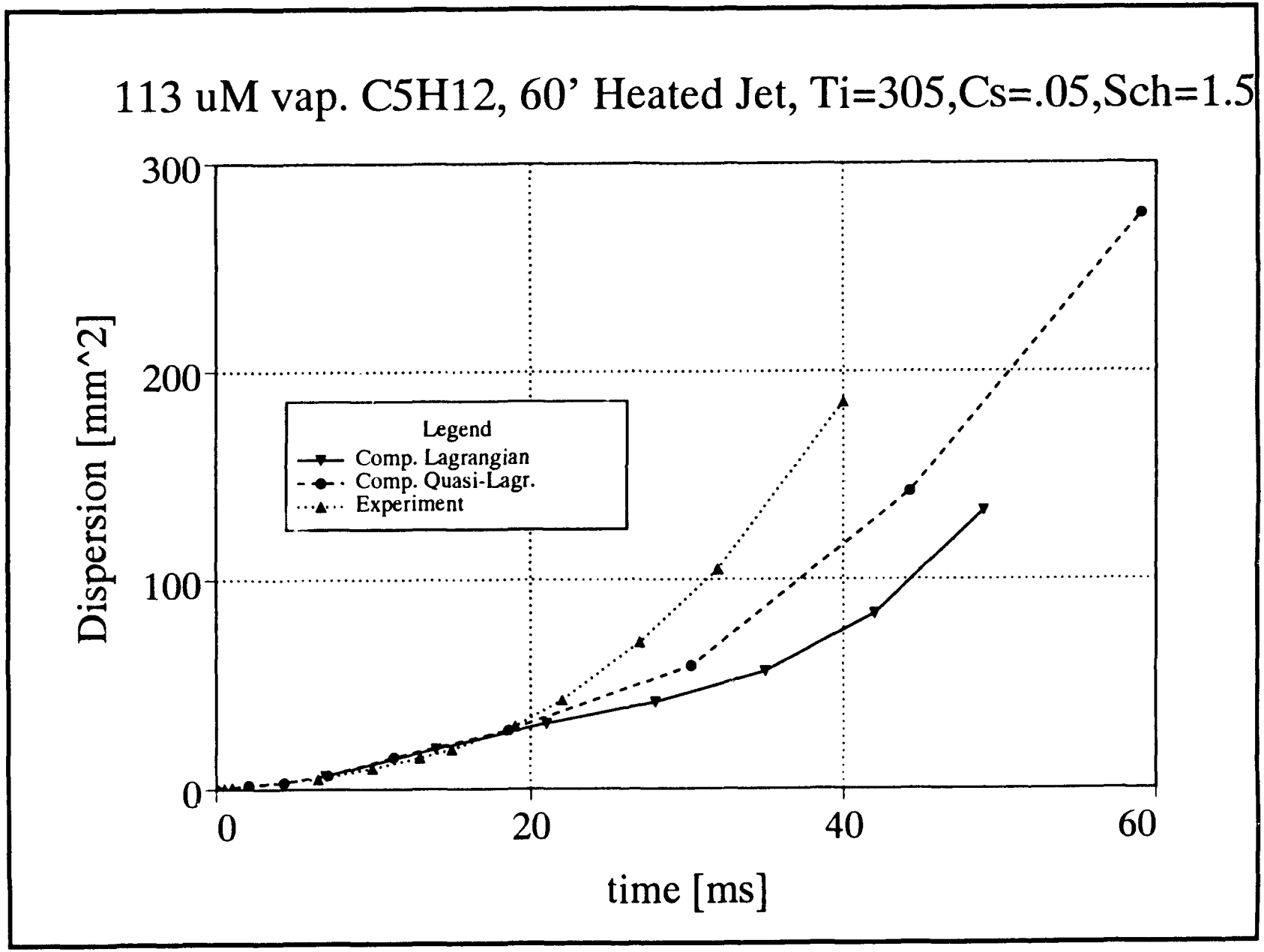
113 uM vap. C5H12, 60' Heated Jet, Ti=305,Cs=.05,Sch=1.5
Dispersion [mm^2]
300
200
100
0
0
20
40
60
time [ms]
Legend
Comp. Lagrangian
Comp. Quasi-Lagr.
Experiment

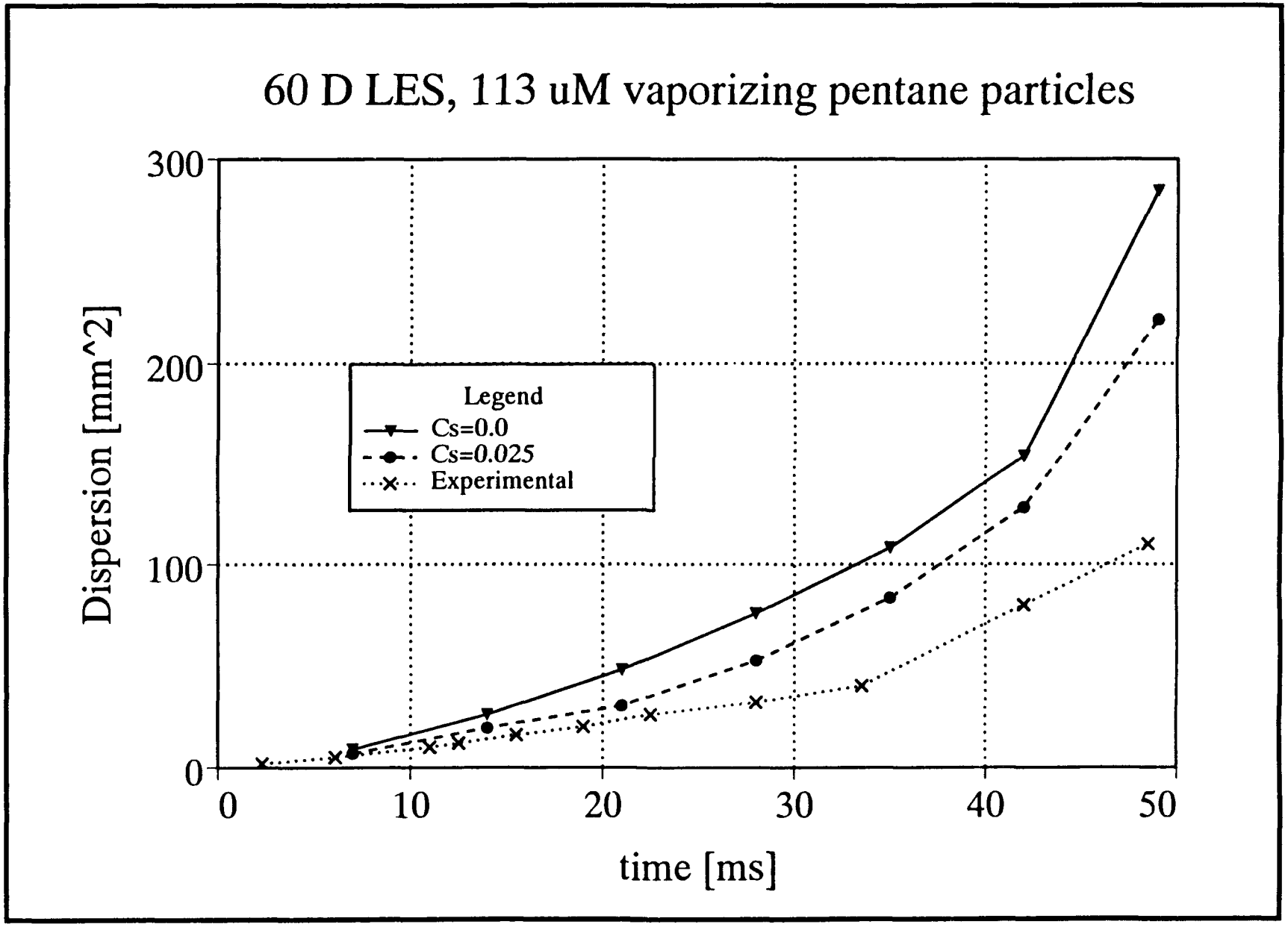
60 D LES, 113 uM vaporizing pentane particles
Dispersion [mm^2]
300
200
100
0
0
10
20
30
40
50
time [ms]
Legend
Cs=0.0
Cs=0.025
Experimental

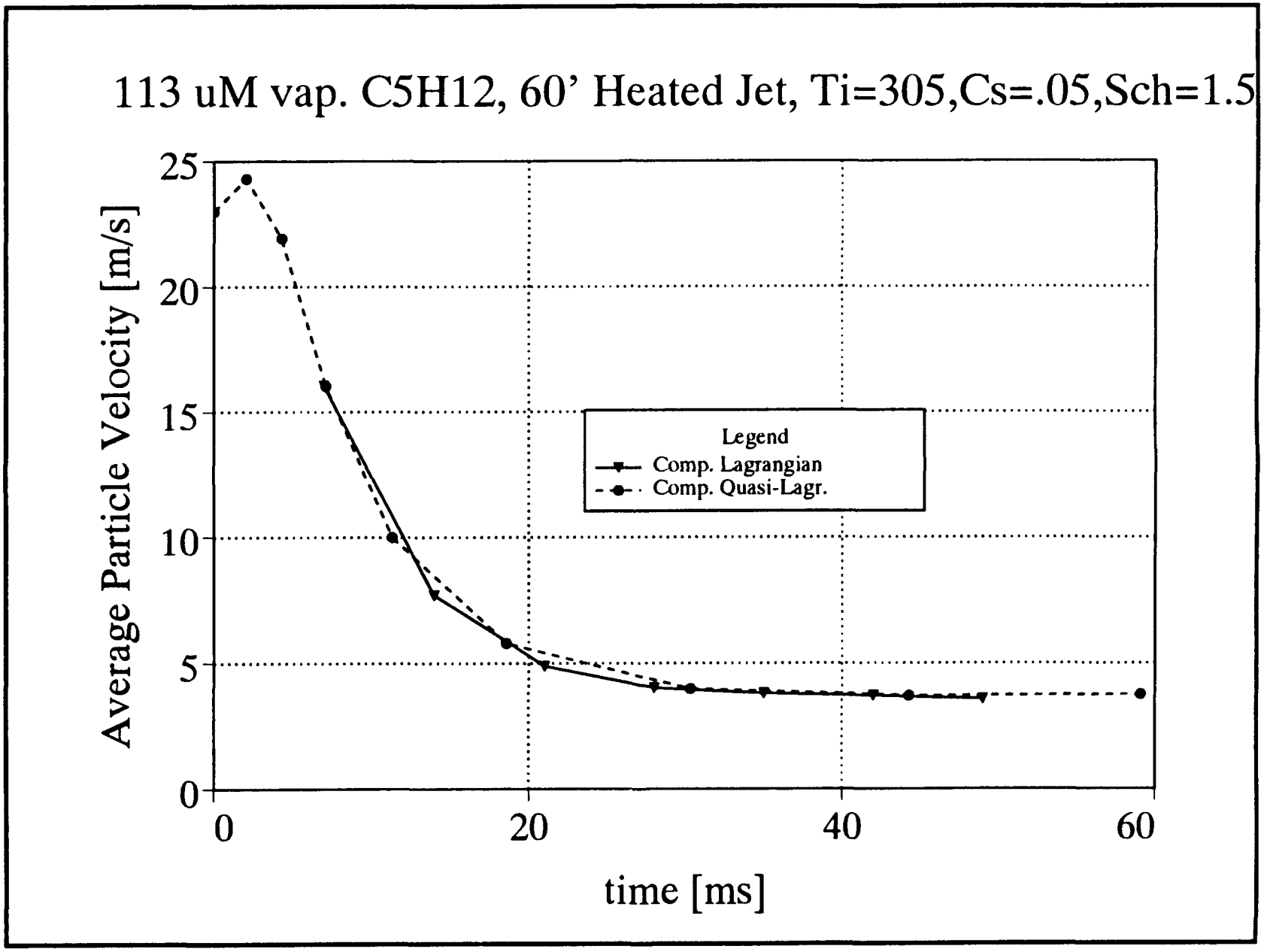
113 uM vap. C5H12, 60' Heated Jet, Ti=305,Cs=.05,Sch=1.5
Average Particle Velocity [m/s]
25
20
15
10
5
0
0
20
40
60
time [ms]
Legend
Comp. Lagrangian
Comp. Quasi-Lagr.

REPORT OF INVENTIONS AND SUBCONTRACTS

(Pursuant to "Patent Rights" Contract Clause) (See Instructions on Reverse Side)

FORM APPROVED OMB NO. 0704-0188

1a. NAME OF CONTRACTOR/ SUBCONTRACTOR	c. CONTRACT NUMBER	2a. NAME OF GOVERNMENT PRIME CONTRACTOR	c. CONTRACT NUMBER	3. TYPE OF REPORT (check one)
University of California	G-F49620-92-J-0418			(X) INTERIM ( ) FINAL
b. ADDRESS (include Zip Code)	d. AWARD DATE (YYMMDD)	b. ADDRESS (include Zip Code)	d. AWARD DATE (YYMMDD)	4. REPORTING PERIOD (YYMMDD)
Davis, CA 95616	920801			FROM 920801 TO 930731

SECTION I - SUBJECT INVENTIONS

5. "SUBJECT INVENTIONS" REQUIRED TO BE REPORTED BY CONTRACTOR/SUBCONTRACTOR (If "None", so state)

a. NAME OF INVENTOR(S) (Last, First, M.I.)	b. TITLE OF INVENTION(S)	c. DISCLOSURE NO., PATENT APPLICATION SERIAL NO. OR PATENT NO.	d. ELECTION TO FILE PATENT APPLICATIONS				e. CONFIRMATORY INSTRUMENT OR ASSIGNMENT FORWARDED TO CONTRACTING OFFICER	
			UNITED STATES		FOREIGN			
			YES	NO	YES	NO	YES	NO
None.								

f. EMPLOYER OF INVENTOR(S) NOT EMPLOYED BY CONTRACTOR/SUBCONTRACTOR.		g. ELECTED FOREIGN COUNTRIES IN WHICH A PATENT APPLICATION WILL BE FILED	
i. NAME OF INVENTOR (Last, First, M.I.)	i. NAME OF INVENTOR (Last, First, M.I.)	i. TITLE OF INVENTION	ii. FOREIGN COUNTRIES OF PATENT APPLICATION
ii. NAME OF EMPLOYER	ii. NAME OF EMPLOYER		
iii. ADDRESS OF EMPLOYER (include Zip Code)	iii. ADDRESS OF EMPLOYER (include Zip Code)		

SECTION II - SUBCONTRACTS (Containing a "Patent Rights" clause)

6. SUBCONTRACTS AWARDED BY CONTRACTOR/SUBCONTRACTOR (If "None", so state)

a. NAME OF SUBCONTRACTOR(S)	b. ADDRESS (include Zip Code)	c. SUBCONTRACT NO.(S)	d. DAR "PATENT RIGHTS"		e. DESCRIPTION OF WORK TO BE PERFORMED UNDER SUBCONTRACT(S)	f. SUBCONTRACT DATES (YYMMDD)	
			CLAUSE NO.	DATE (YYMM)		AWARD	ESTIMATED COMPLETION
None.							

SECTION III - CERTIFICATION

7. CERTIFICATION OF REPORT BY CONTRACTOR/SUBCONTRACTOR (Not required if [ ] Small Business or [ ] Non Profit organization) (Check appropriate box)

a. NAME OF AUTHORIZED CONTRACTOR/SUBCONTRACTOR OFFICIAL (Last, First, M.I.)

b. TITLE

c. I certify that the reporting party has procedures for prompt identification and timely disclosure of "Subject Inventions," that such procedures have been followed and that all "Subject Inventions" have been reported

SIGNATURE OF AUTHORIZED CONTRACTOR/SUBCONTRACTOR OFFICIAL DATE (YYMMDD)

17

Axis treatment of nonsymmetrical flows in cylindrical coordinates

W. Kollmann and J.J. Lienau

MAME Department, University of California at Davis, CA 95616

1.0 Introduction

The turbulent flow in round jets contains a rich variety of structures as documented in experiments (Gutmark et al., 1990, Liepmann, 1991, Yoda et al., 1991, Mungal et al., 1992). Direct and LES simulations of round jets are thus of great importance for the study of the relevant structures in the development of the jet flow. One aspect of such simulations is the treatment of the flow near the axis $r = 0$ in cylindrical coordinates.

The numerical solution of the Navier-Stokes equations in cylindrical coordinates requires the proper treatment of the discretized equations at the axis $r = 0$. The present note is devoted to this aspect of the solution method for flows that possess no particular symmetries. The flow domain is given by $\mathcal{D} = \{(r, \theta, \zeta) : 0 \leq r \leq R_0, 0 \leq \theta \leq 2\pi, 0 \leq \zeta \leq L\}$ with $\partial\mathcal{D}_0 \equiv \{(r, \theta, \zeta) : r = 0, 0 \leq \theta \leq 2\pi, 0 \leq \zeta \leq L\}$ as formally part of the boundary. However, it will be shown that there are no boundary conditions available, but smoothness and uniqueness conditions must be prescribed. The reason for this is the fact that all points in $\partial\mathcal{D}_0$ are inner points. There are two ways to deal with this boundary. The finite difference grid can be staggered such that $r = 0$ is not gridline and no particular action has to be taken, or the Navier-Stokes equations are put into a form suitable for $r = 0$ and smoothness and uniqueness of the dependent variables are enforced. The analysis for the latter case will be carried out and some results for the former case will be presented.

2.0 Navier-Stokes equations in cylindrical coordinates

The method for the solution of the Navier-Stokes equations is based on accurate finite difference schemes. Cylindrical coordinates (r, θ, ζ) appropriate for circular jets are used. Grid stretching is aplied in the r and ζ directions to concentrate the grid points in the region of interest and to remove the outer boundary (R_0 denotes the radial location of the outer boundary) as far as possible without wasting too many grid points (Lienau and Kollmann, 1993). However, the stretching transformation is irrelevant for the analysis of the variation of the dependent variables near the axis $r = 0$ and the standard version of the equations will be considered.

The Navier-Stokes equations for incompressible Newtonian fluids are set up in dimensionless form (The jet pipe radius and the bulk velocity at the entrance section are the reference scales) using cylindrical coordinates. Mass balance emerges then in the form

$$\frac{1}{r}\frac{\partial}{\partial r}(rv_r) + \frac{1}{r}\frac{\partial v_\theta}{\partial \theta} + \frac{\partial v_\zeta}{\partial \zeta} = 0 \tag{1}$$

The radial momentum balance is given by

$$\frac{\partial v_r}{\partial t} + v_r\frac{\partial v_r}{\partial r} + \frac{v_\theta}{r}\frac{\partial v_r}{\partial \theta} + v_\zeta\frac{\partial v_r}{\partial \zeta} - \frac{v_\theta^2}{r} = -\frac{1}{\rho}\frac{\partial p}{\partial r} + \frac{1}{Re}\left\{\frac{\partial}{\partial r}\left(\frac{1}{r}\frac{\partial}{\partial r}(rv_r)\right)\right.$$

$$\left. + \frac{1}{r^2}\frac{\partial^2 v_r}{\partial \theta^2} + \frac{\partial^2 v_r}{\partial \zeta^2} - \frac{2}{r^2}\frac{\partial v_\theta}{\partial \theta}\right\} \tag{2}$$

The azimuthal momentum balance is given by

$$\frac{\partial v_\theta}{\partial t} + v_r\frac{\partial v_\theta}{\partial r} + \frac{v_\theta}{r}\frac{\partial v_\theta}{\partial \theta} + v_\zeta\frac{\partial v_\theta}{\partial \zeta} + \frac{v_\theta v_r}{r} = -\frac{1}{\rho r}\frac{\partial p}{\partial \theta} + \frac{1}{Re}\left\{\frac{\partial}{\partial r}\left(\frac{1}{r}\frac{\partial}{\partial r}(rv_\theta)\right)\right.$$

$$\left. + \frac{1}{r^2}\frac{\partial^2 v_\theta}{\partial \theta^2} + \frac{\partial^2 v_\theta}{\partial \zeta^2} + \frac{2}{r^2}\frac{\partial v_r}{\partial \theta}\right\} \tag{3}$$

Finally, the axial momentum balance is given by

$$\frac{\partial v_\zeta}{\partial t} + v_r\frac{\partial v_\zeta}{\partial r} + \frac{v_\theta}{r}\frac{\partial v_\zeta}{\partial \theta} + v_\zeta\frac{\partial v_\zeta}{\partial \zeta} = -\frac{1}{\rho}\frac{\partial p}{\partial \zeta} + \frac{1}{Re}\left\{\frac{1}{r}\frac{\partial}{\partial r}\left(r\frac{\partial v_\zeta}{\partial r}\right)\right.$$

$$\left. + \frac{1}{r^2}\frac{\partial^2 v_\zeta}{\partial \theta^2} + \frac{\partial^2 v_\zeta}{\partial \zeta^2}\right\} \tag{4}$$

Inspection of mass and momentum balances shows that the limit $r \to 0$ produces singular convective and viscous terms. Hence, a detailed investigation of this limit is called for to make the design of an accurate numerical solution procedure possible.

3.0 The limit $r \to 0$

The analysis of the near axis variation of the dependent variables is based on the assumption that all variables are at least three times continuously differentiable near $r = 0$. Hence we can write

$$p(r,\theta,\zeta) = p(0,\theta,\zeta) + r\frac{\partial p}{\partial r}(0,\theta,\zeta) + \frac{1}{2}r^2\frac{\partial^2 p}{\partial r^2}(0,\theta,\zeta) + O(r^3) \tag{5}$$

and

$$v_\alpha(r,\theta,\zeta) = v_\alpha(0,\theta,\zeta) + r\frac{\partial v_\alpha}{\partial r}(0,\theta,\zeta) + \frac{1}{2}r^2\frac{\partial^2 v_\alpha}{\partial r^2}(0,\theta,\zeta) + O(r^3) \tag{6}$$

valid for $0 \leq r < r_a$ with positive r_a. We consider first the scalar variable p as $r \to 0$. Differentiability at $r = 0$ implies that p must approach the same value as $r \to 0$ for any angle θ and fixed ζ. It follows that the smoothness condition

$$p(0,\theta,\zeta) = p(0,\zeta) \tag{S1}$$

must hold for any scalar variable. This result leads to the pressure gradient at $r = 0$ since differentiation of (5) with respect to θ produces

$$\frac{\partial p}{\partial \theta}(r,\theta,\zeta) = r\frac{\partial^2 p}{\partial r \partial \theta}(0,\theta,\zeta) + \frac{1}{2}r^2\frac{\partial^3 p}{\partial \theta \partial r^2}(0,\theta,\zeta) + O(r^3) \tag{7}$$

and we obtain

$$\nabla p(r,\theta,\zeta) = \begin{pmatrix} \frac{\partial p}{\partial r}(0,\theta,\zeta) \\ \frac{\partial^2 p}{\partial \theta \partial r}(0,\theta\zeta) \\ \frac{\partial p}{\partial \zeta}(0,\theta,\zeta) \end{pmatrix} + \frac{1}{2}r\begin{pmatrix} \frac{\partial^2 p}{\partial \theta \partial r}(0,\theta,\zeta) \\ \frac{\partial^3 p}{\partial \theta \partial r^2}(0,\theta,\zeta) \\ \frac{\partial^2 p}{\partial \theta \partial \zeta}(0,\theta,\zeta) \end{pmatrix} + O(r^2) \tag{8}$$

The smoothness conditions for vectors follow in analogous fashion. The radial velocity component v_r at $r = 0$ becomes the angular component at an angle θ shifted by $\frac{\pi}{2}$ and vice versa. Hence we have the smoothness conditions

$$v_r(0,\theta,\zeta,t) = v_\theta(0,\theta + \frac{\pi}{2},\zeta,t) \tag{S2}$$

and

$$v_\theta(0,\theta,\zeta,t) = v_r(0,\theta - \frac{\pi}{2},\zeta,t) \tag{S3}$$

Furthermore, shifting θ by π reproduces the radial and angular components according to

$$v_r(0,\theta,\zeta,t) = -v_r(0,\theta + \pi,\zeta,t) \tag{S4}$$

and

$$v_\theta(0,\theta,\zeta,t) = -v_\theta(0,\theta + \pi,\zeta,t) \tag{S5}$$

The relations (S2) to (S5) are insufficient to guarantuee smoothness of the velocity projected into the $r-\theta$ plane. This can be seen as follows. Smoothness implies that v_r and v_θ can be expanded in Fourier series at $r=0$

$$v_r(0,\theta) = \sum_{n=0}^{N} a_n^r \exp(i(2n-1)\theta)$$

$$v_\theta(0,\theta) = \sum_{n=0}^{N} a_n^\theta \exp(i(2n-1)\theta)$$

It is easy to see that (S4) and (S5) are satisfied and (S2) and (S3) lead to

$$a_n^\theta = i(-1)^{n+1} a_n^r$$

or

$$a_n^r = i(-1)^n a_n^\theta$$

Hence, v_r determines v_θ at $r=0$ and vice versa. The conditions (S2) to (S5) are thus recognized as periodicity conditions. Consider now the vector $\underline{v}(0,\theta,\zeta,t)$ projected into the $r-\theta$ plane as shown in Fig.1. It is clear that the projection is unique. The projected vector $\underline{v}^p$ can be uniquely decomposed into the orthogonal components v_r and v_θ once the value for the angular coordinate θ has been chosen (see Fig.1).

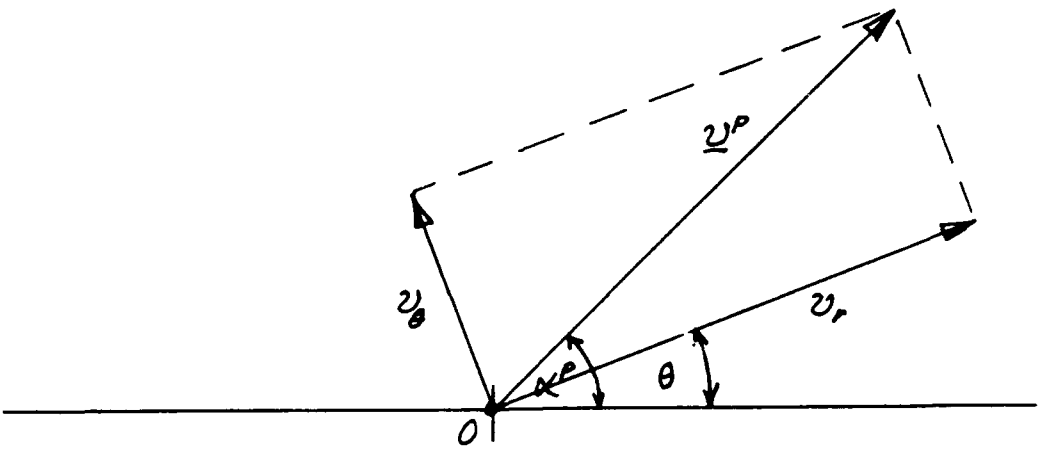

Fig.1. Decomposition of a vector in the $r-\theta$ plane.

It follows that

$$v_r(0,\theta,\zeta,t) = v^p(\zeta,t)\cos(\alpha^p(\zeta,t)-\theta) \qquad (S1^*)$$

and

$$v_\theta(0,\theta,\zeta,t) = v^p(\zeta,t)\sin(\alpha^p(\zeta,t)-\theta) \qquad (S2^*)$$

hold. It is clear that (S1*) and (S2*) imply (S2) to (S5) but the reverse is not true. Several useful relations can be obtained from (S1*) and (S2*) by differentiation. It follows that

$$v_r(0,\theta,\zeta,t) + \frac{\partial v_\theta}{\partial \theta}(0,\theta,\zeta,t) = 0 \tag{10}$$

and

$$v_\theta(0,\theta,\zeta,t) - \frac{\partial v_r}{\partial \theta}(0,\theta,\zeta,t) \tag{11}$$

hold.

Finally, the longitudinal velocity component v_ζ must approach the same limit value as $r \to 0$ no matter what the angular coordinate θ is, hence we have the smoothness condition

$$v_\zeta(0,\theta,\zeta,t) = v_\zeta(0,\zeta,t) \tag{S3*}$$

The following conclusions can be drawn from these considerations: The proper variables decribing the vector $\underline{v}$ at $r = 0$ are $v^p(\zeta,t)$, $\alpha^p(\zeta,t)$ and $v_\zeta(\zeta,t)$. The smoothness conditions (S2) to (S5) are insufficient to determine v^p and α^p uniquely.

3.1 Mass balance

Application of the expansion (6) to (1) leads to

$$\frac{1}{r}\left\{v_r(0) + \frac{\partial v_\theta}{\partial \theta}(0)\right\} + 2\frac{\partial v_r}{\partial r}(0) + \frac{\partial^2 v_\theta}{\partial \theta \partial r}(0) + \frac{\partial v_\zeta}{\partial \zeta}(0) +$$

$$r\left\{\frac{3}{2}\frac{\partial^2 v_r}{\partial r^2}(0) + \frac{1}{2}\frac{\partial^3 v_\theta}{\partial \theta \partial r^2}(0) + \frac{\partial^2 v_\zeta}{\partial \zeta \partial r}(0)\right\} = O(r^2) \tag{12}$$

The solution cannot be smooth as $r \to 0$ unless (10) holds, which takes care of the singularity. Letting $r \to 0$ we get then the proper form of mass balance for $r = 0$

$$2\frac{\partial v_r}{\partial r}(0) + \frac{\partial^2 v_\theta}{\partial \theta \partial r}(0) + \frac{\partial v_\zeta}{\partial \zeta}(0) = 0 \tag{13}$$

If differentiability to higher levels is assumed higher order versions of mass balance for $r = 0$ can be obtained. For instance, applying (10) and (13) to (12), dividing by r and then letting r approach zero leads to

$$\frac{3}{2}\frac{\partial^2 v_r}{\partial r^2}(0) + \frac{1}{2}\frac{\partial^3 v_\theta}{\partial \theta \partial r^2}(0) + \frac{\partial^2 v_\zeta}{\partial \zeta \partial r}(0) = 0 \tag{14}$$

This procedure can be continued to arbitrary levels of differentiability.

3.2 Radial momentum balance

The singular part of the convective terms in (2) is given by

$$C_r \equiv \frac{v_\theta}{r}\left(\frac{\partial v_r}{\partial \theta} - v_\theta\right) \tag{15}$$

Series expansion of the expression in the paranthesis leads to

$$\frac{\partial v_r}{\partial \theta} - v_\theta = \frac{\partial v_r}{\partial \theta}(0) + r\frac{\partial^2 v_r}{\partial \theta \partial r}(0) + \frac{1}{2}r^2\frac{\partial^3 v_r}{\partial \theta \partial r^2}(0) - v_\theta(0) - r\frac{\partial v_\theta}{\partial r}(0) - \frac{1}{2}r^2\frac{\partial^2 v_\theta}{\partial r^2}(0) + O(r^3)$$

The smoothness condition (10) used already to insure the nonsingular character of mass balance leads to

$$\frac{\partial v_r}{\partial \theta} - v_\theta = r\left\{\frac{\partial^2 v_r}{\partial \theta \partial r}(0) - \frac{\partial v_\theta}{\partial r}(0)\right\} + O(r^2) \tag{16}$$

proving the nonsingular properties of convection as $r \to 0$. The singular viscous terms are given by

$$V_r \equiv \frac{\partial}{\partial r}\left(\frac{1}{r}\frac{\partial}{\partial r}(rv_r)\right) + \frac{1}{r^2}\frac{\partial^2 v_r}{\partial \theta^2} - \frac{2}{r^2}\frac{\partial v_\theta}{\partial \theta} \tag{17}$$

Series expansion leads to

$$V_r = \frac{\partial^2 v_r}{\partial r^2} + \frac{1}{r^2}\left(-v_r(0) + \frac{\partial^2 v_r}{\partial \theta^2}(0) - 2\frac{\partial v_\theta}{\partial \theta}(0)\right) + \frac{1}{r}\left(\frac{\partial^3 v_r}{\partial \theta^2 \partial r}(0) - 2\frac{\partial^2 v_\theta}{\partial \theta \partial r}(0)\right)$$
$$+\frac{1}{2}\frac{\partial^2 v_r}{\partial r^2}(0) + \frac{1}{2}\frac{\partial^4 v_r}{\partial \theta^2 \partial r^2}(0) - \frac{\partial^3 v_\theta}{\partial \theta \partial r^2}(0) + O(r)$$

The radial momentum balance should be nonsingular as $r = 0$ is approached which implies that the coefficients of r^{-2} and r^{-1} must vanish. Fist we note that the coefficient of r^{-2} can be recast as

$$-v_r(0) + \frac{\partial^2 v_r}{\partial \theta^2}(0) - 2\frac{\partial v_\theta}{\partial \theta}(0) = -v_r(0) - \frac{\partial v_\theta}{\partial \theta}(0) + \frac{\partial}{\partial \theta}\left(\frac{\partial v_r}{\partial \theta}(0) - v_\theta(0)\right)$$

Smoothness as $r \to 0$ requires that (10) and (11) hold, which implies that the coefficient of r^{-2} vanishes. The coefficient of r^{-1} can be rearranged as

$$\frac{\partial^3 v_r}{\partial \theta^2 \partial r}(0) - 2\frac{\partial^2 v_\theta}{\partial \theta \partial r}(0) = \frac{\partial}{\partial \theta}\left(\frac{\partial^2 v_r}{\partial \theta \partial r}(0) - 2\frac{\partial v_\theta}{\partial r}(0)\right)$$

The radial momentum balance would be singular if this coefficient was nonzero. We conclude that

$$\frac{\partial^2 v_r}{\partial \theta \partial r}(0) - 2\frac{\partial v_\theta}{\partial r}(0) = \mathcal{F}(\zeta, t) \tag{18}$$

insures nonsingularity. The radial momentum balance for $r = 0$ emerges now in the form

$$\frac{\partial v_r}{\partial t} + v_r\frac{\partial v_r}{\partial r} + v_\theta\frac{\partial^2 v_r}{\partial \theta \partial r} + v_\zeta\frac{\partial v_r}{\partial \zeta} - v_\theta\frac{\partial v_\theta}{\partial r} = -\frac{1}{\rho}\frac{\partial p}{\partial r} + \frac{1}{Re}\left\{\frac{3}{2}\frac{\partial^2 v_r}{\partial r^2}\right.$$
$$\left. + \frac{\partial^4 v_r}{\partial \theta^2 \partial r^2} + \frac{\partial^2 v_r}{\partial \zeta^2} - 2\frac{\partial^3 v_\theta}{\partial \theta \partial r^2}\right\} \tag{19}$$

strictly valid for $r = 0$.

3.3 Angular momentum balance

The singular part of the convective terms in (3) is given by

$$C_\theta \equiv \frac{v_\theta}{r}\left(\frac{\partial v_\theta}{\partial \theta} + v_r\right) \tag{20}$$

Series expansion of the expression in the paranthesis leads to

$$\frac{\partial v_theta}{\partial \theta} + v_r = \frac{\partial v_\theta}{\partial \theta}(0) + v_r(0) + r\left\{\frac{\partial^2 v_\theta}{\partial \theta \partial r}(0) + \frac{\partial v_r}{\partial r}(0)\right\} + O(r^2)$$

The smoothness condition (10) leads to

$$\frac{\partial v_\theta}{\partial \theta} + v_r = r\left\{\frac{\partial^2 v_\theta}{\partial \theta \partial r}(0) + \frac{\partial v_r}{\partial r}(0)\right\} + O(r^2) \tag{21}$$

proving the nonsingular properties of convection as $r \to 0$. The (scalar variable) pressure can be expanded and we get according to (5)

$$\frac{1}{r}\frac{\partial p}{\partial \theta} = \frac{\partial^2 p}{\partial \theta \partial r}(0) + O(r)$$

The singular viscous terms are given by

$$V_\theta \equiv \frac{\partial}{\partial r}\left(\frac{1}{r}\frac{\partial}{\partial r}(r v_\theta)\right) + \frac{1}{r^2}\frac{\partial^2 v_\theta}{\partial \theta^2} + \frac{2}{r^2}\frac{\partial v_r}{\partial \theta} \tag{22}$$

Series expansion leads to

$$V_\theta = \frac{\partial^2 v_\theta}{\partial r^2} + \frac{1}{r^2}\left(-v_\theta(0) + \frac{\partial^2 v_\theta}{\partial \theta^2}(0) + 2\frac{\partial v_r}{\partial \theta}(0)\right) + \frac{1}{r}\left(\frac{\partial^3 v_\theta}{\partial \theta^2 \partial r}(0) + 2\frac{\partial^2 v_r}{\partial \theta \partial r}(0)\right)$$

$$+\frac{1}{2}\frac{\partial^2 v_\theta}{\partial r^2}(0) + \frac{1}{2}\frac{\partial^4 v_\theta}{\partial \theta^2 \partial r^2}(0) + \frac{\partial^3 v_r}{\partial \theta \partial r^2}(0) + O(r)$$

The angular momentum balance should be nonsingular as $r = 0$ is approached which implies that the coefficients of r^{-2} and r^{-1} must vanish. Fist we note that the coefficient of r^{-2} can be recast as

$$-v_\theta(0) + \frac{\partial^2 v_\theta}{\partial \theta^2}(0) + 2\frac{\partial v_r}{\partial \theta}(0) = -v_\theta(0) + \frac{\partial v_r}{\partial \theta}(0) + \frac{\partial}{\partial \theta}\left(\frac{\partial v_\theta}{\partial \theta}(0) + v_r(0)\right)$$

Smoothness as $r \to 0$ requires that (10) and (11) hold which implies that the coefficient of r^{-2} vanishes. The coefficient of $r-1$ can be rearranged as

$$\frac{\partial^3 v_\theta}{\partial \theta^2 \partial r}(0) + 2\frac{\partial^2 v_r}{\partial \theta \partial r}(0) = \frac{\partial}{\partial \theta}\left(\frac{\partial^2 v_\theta}{\partial \theta \partial r}(0) + 2\frac{\partial v_r}{\partial r}(0)\right)$$

The angular momentum balance would be singular if this coefficient was nonzero. We conclude that

$$\frac{\partial^2 v_\theta}{\partial\theta\partial r}(0) + 2\frac{\partial v_r}{\partial r}(0) = \mathcal{F}(\zeta, t) \tag{23}$$

insures nonsingularity. The angular momentum balance for $r = 0$ emerges now in the form

$$\frac{\partial v_\theta}{\partial t} + v_r\frac{\partial v_\theta}{\partial r} + v_\theta\frac{\partial^2 v_\theta}{\partial\theta\partial r} + v_\zeta\frac{\partial v_\theta}{\partial\zeta} + v_\theta\frac{\partial v_r}{\partial r} = -\frac{1}{\rho}\frac{\partial^2 p}{\partial\theta\partial r} + \frac{1}{Re}\left\{3/over2\frac{\partial^2 v_\theta}{\partial r^2}\right.$$
$$\left. + \frac{\partial^4 v_\theta}{\partial\theta^2\partial r^2} + \frac{\partial^2 v_\theta}{\partial\zeta^2} - 2\frac{\partial^3 v_r}{\partial\theta\partial r^2}\right\} \tag{24}$$

strictly valid for $r = 0$.

3.4 Longitudinal momentum balance

The singular part of the convective terms in (4) is a single term which can be expanded as

$$\frac{v_\theta}{r}\frac{\partial v_\zeta}{\partial\theta} = \frac{v_\theta}{r}\left\{\frac{\partial v_\zeta}{\partial\theta}(0) + r\frac{\partial^2 v_\zeta}{\partial\theta\partial r}(0) + O(r^2)\right\} \tag{25}$$

Smoothness of v_ζ as $r \to 0$ requires that $v_\zeta(0, \theta, \zeta, t)$ is independent of the angular variable θ, hence we conclude that

$$\frac{v_\theta}{r}\frac{\partial v_\zeta}{\partial\theta} = v_\theta\frac{\partial^2 v_\zeta}{\partial\theta\partial r}(0) + O(r) \tag{27}$$

holds. The singular viscous terms are given by

$$V_\zeta \equiv \frac{1}{r}\frac{\partial}{\partial r}\left(r\frac{\partial v_\zeta}{\partial r}\right) + \frac{1}{r^2}\frac{\partial^2 v_\zeta}{\partial\theta^2} \tag{27}$$

Series expansion leads to

$$V_\zeta = \frac{1}{r^2}\frac{\partial^2 v_\zeta}{\partial\theta^2}(0) + \frac{1}{r}\left(\frac{\partial^3 v_\zeta}{\partial\theta^2\partial r}(0) + \frac{\partial v_\zeta}{\partial r}(0)\right)$$
$$+2\frac{\partial^2 v_\zeta}{\partial r^2}(0) + \frac{1}{2}\frac{\partial^4 v_\zeta}{\partial\theta^2\partial r^2}(0) + O(r)$$

The longitudinal momentum balance should be nonsingular as $r = 0$ is approached which implies that the coefficients of r^{-2} and r^{-1} must vanish. Fist we note that the coefficient of r^{-2} vanishes since $v_\zeta(0, \theta, \zeta, t)$ must be independent of θ according to (S3*). The coefficient of r^{-1} must also vanish, hence we require

$$\frac{\partial^3 v_\zeta}{\partial\theta^2\partial r}(0) + \frac{\partial v_\zeta}{\partial r}(0) = 0 \tag{28}$$

to insure nonsingularity. The longitudinal momentum balance for $r = 0$ emerges now in the form

$$\frac{\partial v_\zeta}{\partial t} + v_r\frac{\partial v_\zeta}{\partial r} + v_\theta\frac{\partial^2 v_\zeta}{\partial\theta\partial r} + v_\zeta\frac{\partial v_\zeta}{\partial\zeta} = -\frac{1}{\rho}\frac{\partial p}{\partial\zeta} + \frac{1}{Re}\left\{2\frac{\partial^2 v_\zeta}{\partial r^2}\right.$$
$$\left. + \frac{1}{2}\frac{\partial^4 v_\zeta}{\partial\theta^2\partial r^2} + \frac{\partial^2 v_\zeta}{\partial\zeta^2}\right\} \tag{29}$$

strictly valid for $r = 0$.

3.5 Navier-Stokes equations at $r = 0$

The results of the previous section provide the proper form of the Navier-Stokes equations for points on the grid surface $\partial\mathcal{D}_0$. We summarize the equations first and then discuss a possible strategy for the solution. Mass balance for $r = 0$ is according to section 3.1 given by

$$2\frac{\partial v_r}{\partial r}(0) + \frac{\partial^2 v_\theta}{\partial\theta\partial r}(0) + \frac{\partial v_\zeta}{\partial\zeta}(0) = 0$$

The momentum balance in radial direction is according to section 3.2

$$\frac{\partial v_r}{\partial t} + v_r\frac{\partial v_r}{\partial r} + v_\theta\frac{\partial^2 v_r}{\partial\theta\partial r} + v_\zeta\frac{\partial v_r}{\partial\zeta} - v_\theta\frac{\partial v_\theta}{\partial r} = -\frac{1}{\rho}\frac{\partial p}{\partial r} + \frac{1}{Re}\left\{\frac{3}{2}\frac{\partial^2 v_r}{\partial r^2}\right.$$

$$\left. + \frac{\partial^4 v_r}{\partial\theta^2\partial r^2} + \frac{\partial^2 v_r}{\partial\zeta^2} - 2\frac{\partial^3 v_\theta}{\partial\theta\partial r^2}\right\}$$

The angular momentum balance is not needed, as will be shown below, and the axial momentum balance is according to section 3.4 given by

$$\frac{\partial v_\zeta}{\partial t} + v_r\frac{\partial v_\zeta}{\partial r} + v_\theta\frac{\partial^2 v_\zeta}{\partial\theta\partial r} + v_\zeta\frac{\partial v_\zeta}{\partial\zeta} = -\frac{1}{\rho}\frac{\partial p}{\partial\zeta} + \frac{1}{Re}\left\{2\frac{\partial^2 v_\zeta}{\partial r^2}\right.$$

$$\left. + \frac{1}{2}\frac{\partial^4 v_\zeta}{\partial\theta^2\partial r^2} + \frac{\partial^2 v_\zeta}{\partial\zeta^2}\right\}$$

The smoothness and uniqueness conditions obtained in section 3.0 can be applied as follows: The velocity vector at $r = 0$ projected into the $r - \theta$ plane is determined by v^p and α^p and solving the radial momentum balance at $r = 0$ for $\theta = 0$ and $\theta = \frac{\pi}{2}$ leads to

$$v_r(0, 0, \zeta, t) = v^p(\zeta, t)\cos(\alpha^p(\zeta, t)) \tag{30}$$

and

$$v_r(0, \frac{\pi}{2}, \zeta, t) = v^p(\zeta, t)\sin(\alpha^p(\zeta, t)) \tag{31}$$

Hence we get

$$v^p(\zeta, t) = \sqrt{v_r^2(0, 0, \zeta, t) + v_r^2(0, \frac{\pi}{2}, \zeta, t)} \tag{32}$$

and

$$\alpha^p(\zeta, t) = \arctan\left(\frac{v_r(0, \frac{\pi}{2}, \zeta, t)}{v_r(0, 0, \zeta, t)}\right) \tag{33}$$

for the projected velocity at $r = 0$. Once v^p and α^p have been determined the radial and angular velocity components at $r = 0$ follow from (S1*) and (S2*).

The strategy for the solution includes the following steps to deal with the axis $r = 0$: Solve mass balance (13), the axial momentum balance (29) and the radial momentum balance

(19) for $\theta = 0$ and $\theta = \frac{\pi}{2}$. Then we obtain the projected velocity vector from (32) and (33). The radial and circumferential velocity components follow then from (S1*) and (S2*) as

$$v_r(0,\theta,\zeta,t) = \sqrt{v_r^2(0,0,\zeta,t) + v_r^2(0,\frac{\pi}{2},\zeta,t)}\cos(\arctan\left(\frac{v_r(0,\frac{\pi}{2},\zeta,t)}{v_r(0,0,\zeta,t)}\right) - \theta) \qquad (34)$$

and

$$v_\theta(0,\theta,\zeta,t) = \sqrt{v_r^2(0,0,\zeta,t) + v_r^2(0,\frac{\pi}{2},\zeta,t)}\sin(\arctan\left(\frac{v_r(0,\frac{\pi}{2},\zeta,t)}{v_r(0,0,\zeta,t)}\right) - \theta) \qquad (35)$$

This completes the treatment of the axis if $r = 0$ is gridline.

4.0 Application

The finite-difference method described by Lienau and Kollmann (1993) was applied to the prediction of the flow in a round jet for a nominal Reynolds number of $Re = 15000$. The development of the axial and circumferential instabilities leads quickly to solutions without symmetries, hence requirung the proper treatment of the dependent variables near the axis $r = 0$. Two treatments of the axis are considered:

(1) The grid contains $r = 0$ as gridline and the smoothness conditions (S1) to (S5) are enforced but not the uniqueness conditions (S1*) to (S3*).

(2) The grid is staggered and $r = 0$ is not gridline.

The results for case (1) in Fig.2 for velocity and in Fig.3 for vorticity show that spurious higher harmonics in circumferential direction appear and are insufficiently damped. The solution remains bounded but the near axis variation of velocity and vorticity are unsatisfactory. The results for the case (2) in Fig.4 for velocity and in Fig.5 for vorticity on the other hand are quite satisfactory.

5.0 Conclusions.

A finite difference method for the Navier-Stokes equations in cylindrical coordinates was developed that is sixth order accurate in space and second order accurate in time. The treatment of the dependent variables and the structure of the Navier-Stokes near $r = 0$ was established using series expansions and the conditions that variables and equations must remain nonsingular and unique for $r \to 0$. The application of two different treatments of the axis $r = 0$ lead to the conclusion that staggered grids are superior over non-staggered grids, where the enforcement of smoothness is not sufficient to produce satisfactory results. It is clear that uniqueness conditions should be imposed in this case, but this has not yet been tested.

References.

Gutmark, E., Parr, T.P., Hanson-Parr, D.M. and Schadow, K.C. (1990), "Coherent and random structure in reacting jets", Experim. in Fluids **10**, 147.

Lele, S.K. (1990), "Compact finite-difference schemes with spectral-like resoltion", CTR manuscript 107.

Lienau, J.J. and Kollmann, W. (1993), "Numerical simulation of the turbulent flow in round jets", AIAA Paper 93-0199.

Liepmann, D. (1991), "Streamwise vorticity and entrainment in the near field of a round jet", Phys. Fluids A **3**, 1179.

Martin, J.E. and Meiburg, E. (1991), "Numerical investigation of three-dimensionally evolving jets subject to axisymmetric and azimuthal perturbations", J. Fluid Mech. **230**, 271.

Melander, M.V., Hussain, F. and Basu, A. (1991), "Breakdown of a circular jet into turbulence", Proc. 8th Symp. Turbulent Shear Flows, Munich, Germany, 15-5-1.

Mungal, M.G., Lozano, A. and Van Cruyningen, I. (1992), "Large-scale dynamics in high Reynolds number jets and jet flames", Experim. in Fluids **12**, 141.

Rai, M.M. and Moin, P. (1991), "Direct simulations of turbulent flow using finite-difference schemes", J. Comput. Physics **96**, 15.

Yoda, M., Hesselink, L. and Mungal, M.G. (1991), "The temporal evolution of large-scale structures in the turbulent jet", Proc. 8th Symp. Turbulent Shear Flows, Munich, Germany, 6-1-1.

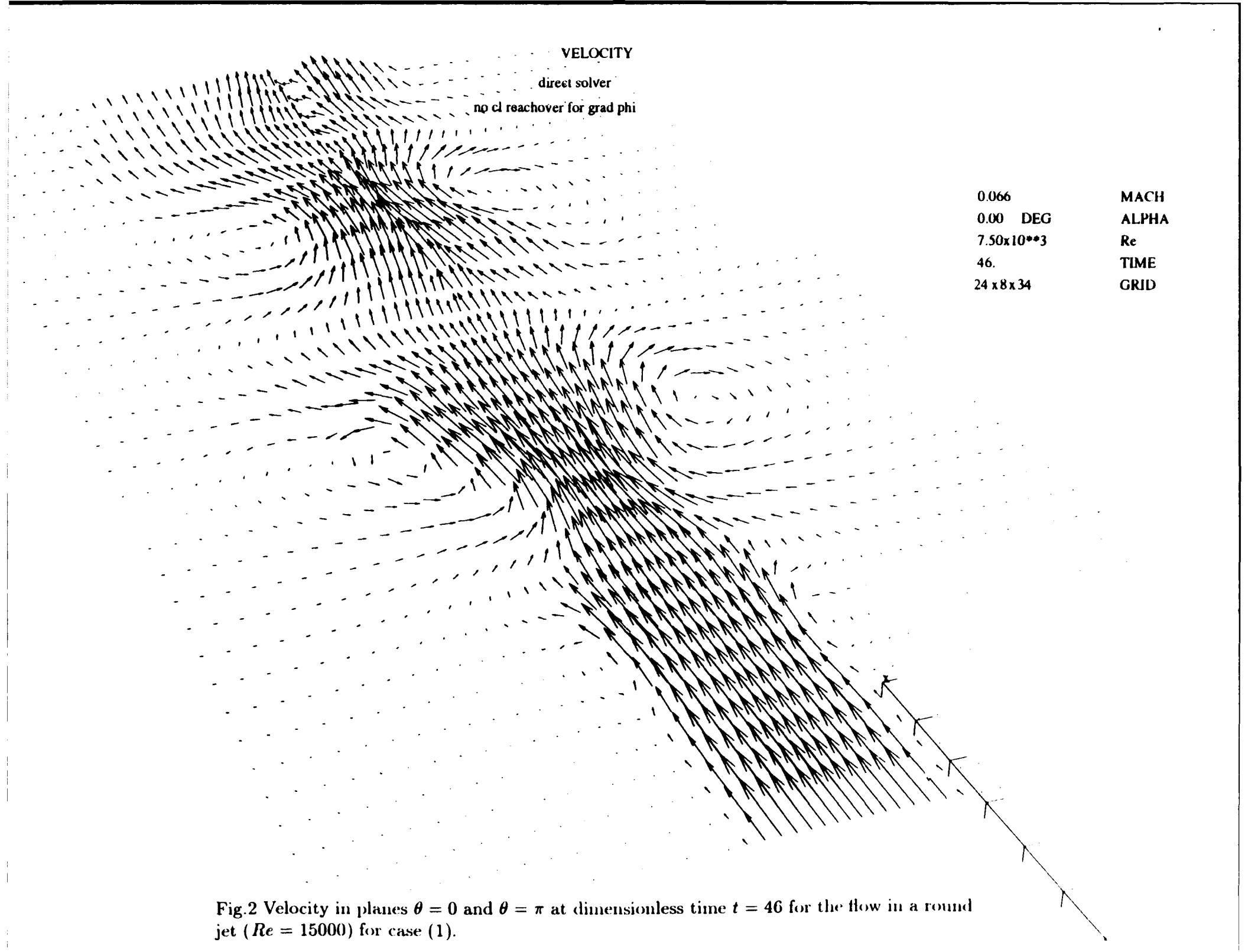

Fig.2 Velocity in planes $\theta = 0$ and $\theta = \pi$ at dimensionless time $t = 46$ for the flow in a round jet ($Re = 15000$) for case (1).

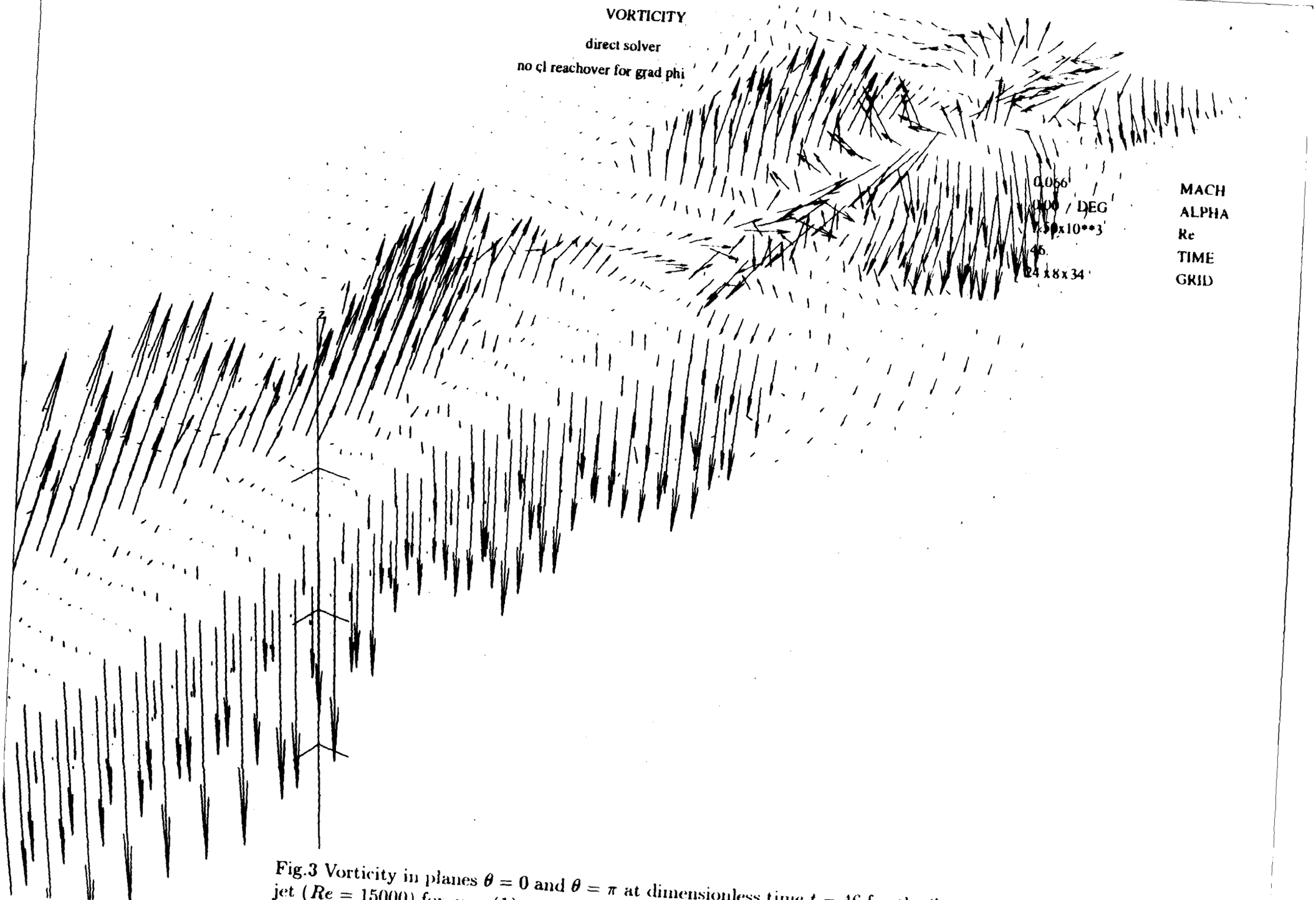

Fig.3 Vorticity in planes $\theta = 0$ and $\theta = \pi$ at dimensionless time $t = 46$ for the flow in a round jet ($Re = 15000$) for case (1).

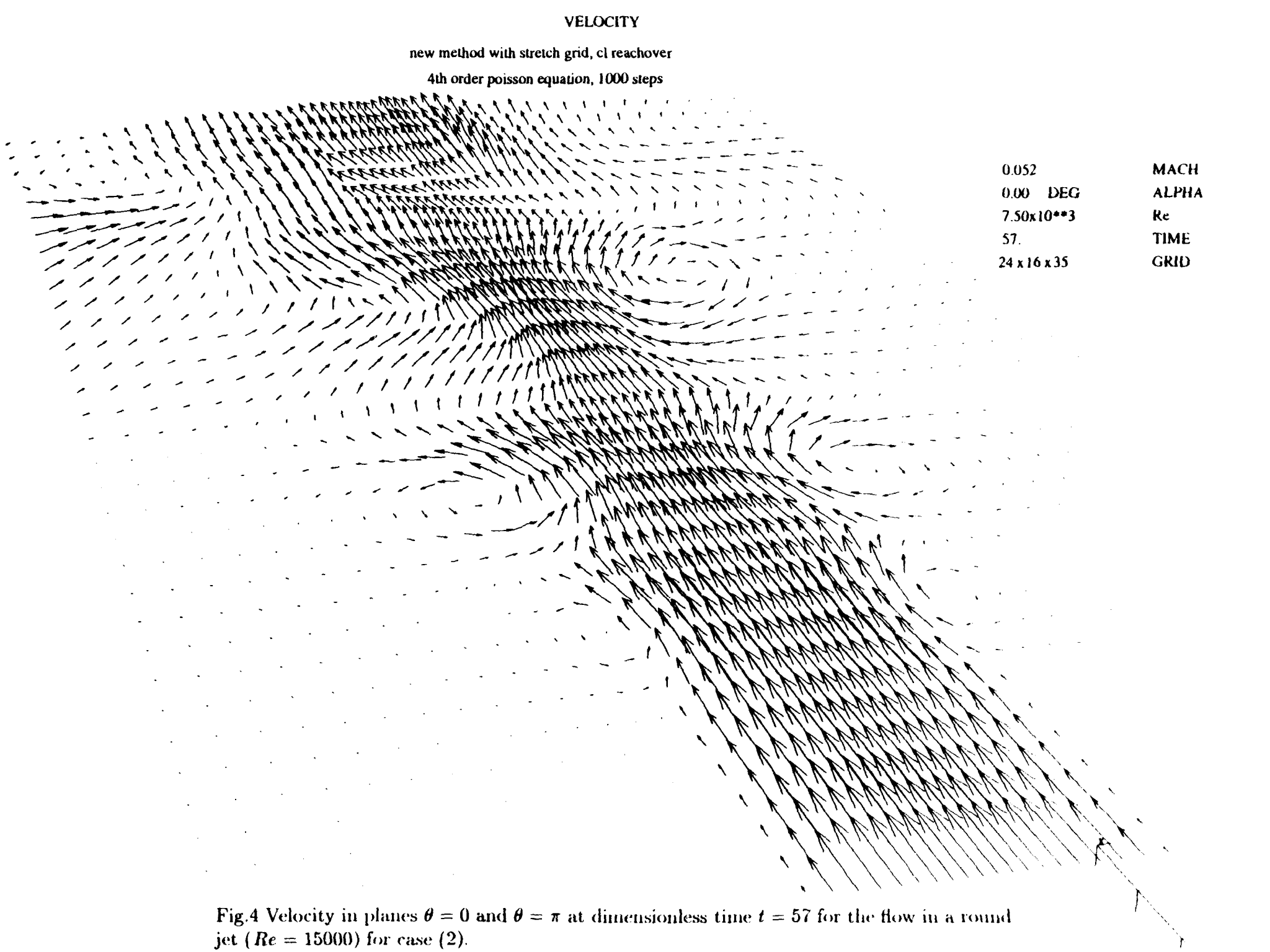

Fig.4 Velocity in planes $\theta = 0$ and $\theta = \pi$ at dimensionless time $t = 57$ for the flow in a round jet ($Re = 15000$) for case (2).

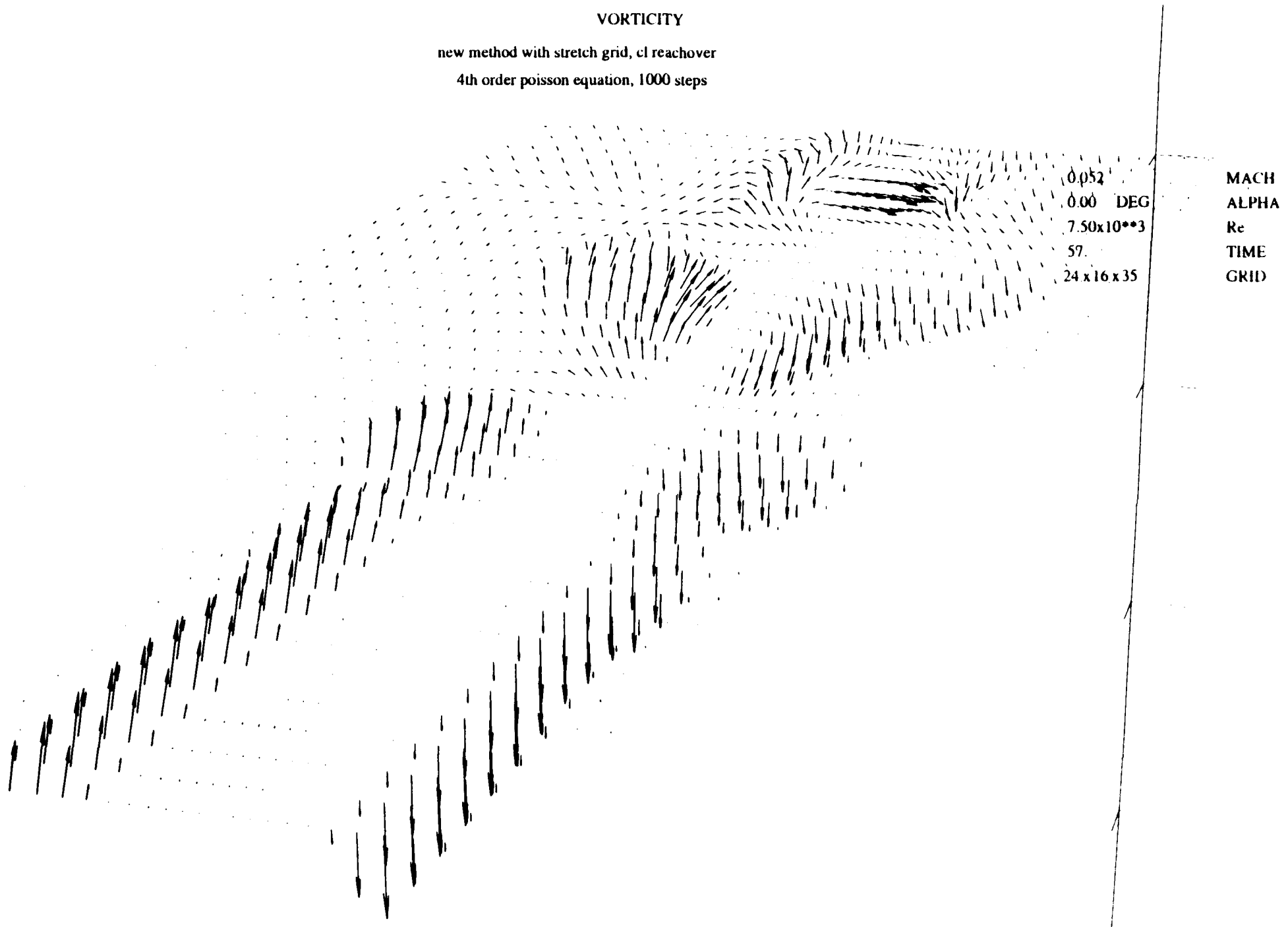

Fig.5 Vorticity in planes $\theta = 0$ and $\theta = \pi$ at dimensionless time $t = 57$ for the flow in a round jet ($Re = 15000$) for case (2).